10.1109/ULTSYM.2012.0351

# Photoacoustic measurements of single red blood cells

Eric M. Strohm, Eno Hysi, Michael C. Kolios
Department of Physics
Ryerson University
Toronto, Ontario, Canada
mkolios@ryerson.ca

*Abstract*— **A photoacoustic method to infer the size, shape and orientation of single RBCs is presented. Diseased or damaged RBCs frequently have abnormal shapes and sizes, which can result from a variety of diseases. When using frequencies between 100 and 500 MHz, the photoacoustic power spectrum from RBCs has periodically varying minima and maxima that depend on the size and shape of the RBC. The signals from RBCs in a vertical and horizontal orientation relative to the transducer were compared to numerical simulations using a finite element model. Three different shapes commonly used to model RBCs were examined (at constant volume): a biconcave disk, an oblate ellipsoid and a sphere. For a single biconcave shaped RBC, good agreement in the shape of the power spectrum was observed between measured and numerical simulations for the RBC in both the vertical and horizontal orientation relative to the transducer. When the RBC was placed in a hypotonic solution, it swelled to a spherical shape. In this case, good agreement was observed between the measured signal and the spherical model. In this paper, we show that the photoacoustic power spectrum can be used to infer the size, shape and orientation of single RBCs.**

## I. Introduction

Red blood cells (RBCs) have a biconcave shape that enables efficient transport through narrow capillaries, and increases the surface area for maximizing oxygen transport. The average RBC diameter is 7.82 μm with a mean surface area of 135 $\mu m^3$ and mean volume of 94 $\mu m^3$ [1]. RBC abnormalities can alter the cell elastic properties, resulting in changes to the size, volume and surface area, ultimately leading to reduced oxygen transport and blood flow efficiency. Abnormalities in the RBC size or shape can occur through trauma, disease such as spherocytosis or sickle cell disease, infection such as malaria, anemia, or changes in the surrounding blood chemistry [2].

Clinical diagnosis of blood-related disease uses methods to detect changes in the mean RBC size and volume. Accepted blood analysis techniques include blood smear analysis, dynamic light scattering and electrical impedance [2]. Other techniques that can be used to probe for RBC dysfunction include optical speckle analysis [3], spectroscopic methods [4], and ultrasound backscatter [5]. The hemoglobin within RBCs has strong optical absorption in the visible wavelengths, enabling photoacoustic measurements using the RBC endogenous contrast. Photoacoustic methods have been developed to image RBCs [6][7], however these methods are unable to detect their shape and structure. We propose using a photoacoustic method to determine the size and morphology of RBCs by examining the power spectrum over the frequency range of 100-500 MHz. When irradiated with a laser, the RBCs emit a photoacoustic wave with a characteristic power spectrum that has periodically-varying periodic minima and maxima that depend on the size, shape and acoustic properties such as the sound speed of that RBC [8].

The measurements of single RBCs are compared to numerical simulations developed using a finite element model (FEM). The unique biconcave shape of RBCs is frequently modeled as a sphere or an oblate ellipsoid for computational efficiency [9][10], however these approximations can give erroneous results due to the over-simplification of their structure. This paper explores the photoacoustic power spectrum emitted from single RBCs as a function of orientation and shape. The signals are then compared to FEM simulations using the biconcave, spherical and oblate morphologies to determine the accuracy of using simpler geometries for modeling.

## II. Materials and Methods

### A. Photoacoustic Microscope

A SASAM photoacoustic microscope (Kibero GmbH Germany) was used to record the photoacoustic signals from the RBCs. It consists of an Olympus IX81 optical microscope (Olympus, Japan), and a transducer that is positioned above the sample holder. The sample was irradiated with a 532 nm laser (Teem Photonics, France) focused to a 10 μm spot diameter using a 10x optical objective. The optical view enabled precise sample targeting and alignment of the transducer to the laser. The system was maintained at a constant temperature of 36ºC. The laser pulse width was 330 ps with a repetition frequency of 4 kHz, and the fluence was adjustable to between 10 to 100 $mJ/cm^2$ using an optical attenuator. A 375 MHz transducer (f/1, 42% -6 dB bandwidth) was used for all measurements. Signals were amplified by a 40 dB amplifier (Miteq, USA) and digitized at 8 GS/s. A Hamming window and bandpass filter of 100-800 MHz was applied to all measurements. The signals were normalized by removing the transducer response. Specific details of the system construction and signal processing methods can be found elsewhere [11][12].

### B. Measurements

RBCs were extracted from a healthy male volunteer via a finger prick. This procedure was approved by the Ryerson Ethics Board (#2012-210), and informed consent was obtained from the volunteer. The extracted RBCs were immediately

diluted in a solution containing Dulbecco's modified Eagle's Medium (DMEM) with 10% fetal bovine serum (FBS) to maintain viability. The RBCs were then deposited onto a glass-bottom petri-dish (Mattek Corporation, USA) that contained a thin layer of agar (0.5% concentration). The agar was used to reduce back reflections from the glass substrate under the RBC. Within a few minutes of inserting the RBCs into the coupling medium, most settled onto the bottom in a "horizontal" orientation, however some aligned vertically on their edge as shown in figure 1. Within a time period of a few minutes, the vertical RBCs would fall over onto their side. The photoacoustic signal was recorded as the RBC rotated from a vertical to horizontal orientation. The RBC diameter was obtained from the optical images and was used in the numerical simulations.

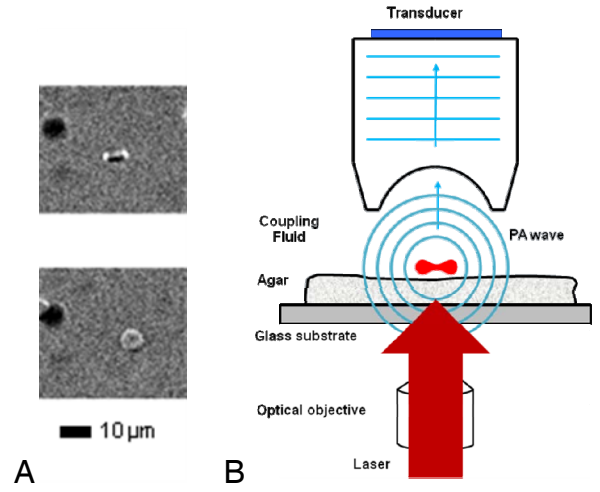


Figure 1. (A) Optical images of the same RBC in a vertical (top) and horizontal orientation (bottom) (B). A schematic showing how the photoacoustic signal from a single RBC was measured.

### C. *Numerical Simulations*

A 2D axisymmetric FEM was developed using COMSOL Multiphysics (Stockholm, Sweden). The model was initiated immediately after the RBC was irradiated with the laser, but before acoustic propagation occurred. To simulate the increase in pressure in the RBC that occurs after laser irradiation, the pressure of the irradiated RBC was set to unity and the surrounding coupling fluid pressure was set to zero. The model assumes the RBC absorbed the laser energy uniformly and instantaneously, and was within thermal and stress confinement conditions. The transient acoustics module was used to calculate the photoacoustic waves from the RBC. Specifically, the wave equation was solved to calculate the acoustic propagation resulting from the pressure differential between the RBC and coupling fluid.

The equation describing an average-sized RBC (7.82 µm diameter, 94 $\mu m^3$) that was developed by Fung *et al.* was used to model the RBC shape [1]. The density and sound speed of the RBC and coupling fluid must be known for accurate simulations. The density of single human RBCs ranges from 1090 to 1110 $kg/m^3$ [9][13]; we used in our simulations 1100 $kg/m^3$. The sound speed of single RBCs is not well known. The sound speed of a 95% weight fraction of blood was 1620 m/s, and extrapolating to 100% yielded 1700 m/s [14]. In our simulations, we used 1650 m/s. The coupling fluid sound speed and density were 1520 m/s and 1000 $kg/m^3$, respectively. The outer boundary was set to a radius of 10 µm. The locations at which the pressure profiles were recorded were around the outer boundary (emulating the locations of transducers). The numerical solutions took approximately 4 hours to solve using a 0.05 µm mesh with nearly 600,000 degrees of freedom. Solutions to the wave propagation were output at time steps of 0.0625 ns. Simulations of RBCs frequently use an oblate ellipsoid or a spheroid due to the computational overhead required in solving a non-symmetric bi-concave shape. FEM solutions using an oblate and spheroid model were calculated to compare the accuracy of these geometries to the bi-concave shape. The major and minor axes of the oblate were 3.91 µm and 1.47 µm, respectively, while the spherical model was 2.82 µm in radius (figure 2).

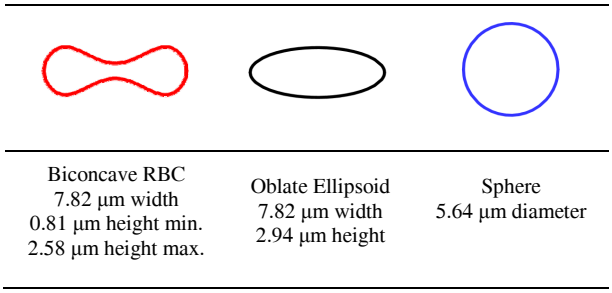


Figure 2. The shape and dimenional parameters used for the three morphologies studied in the numerical simulation. All shapes had the same volume of 94 $\mu m^3$.

## III. Results and Discussion

The FEM was solved for an average RBC size (7.82 µm, 94 $\mu m^3$) as shown in figure 3A. During the simulation, the transient acoustic signal was recorded over time at locations around the system boundary to investigate how the signals vary in relation to the RBC orientation. The power spectrum of these signals is shown in figure 3B for angles of 0, 30, 60 and 90° relative to the RBC. As the location of the transducer was rotated from the 0° position (RBC edge towards the transducer) to 90° (RBC flat section towards the transducer), the spectral minima and maxima shifted to higher frequencies. The first spectral minimum that occurs at 220 MHz for a 90° orientation slowly shifted to higher frequencies, reaching 730 MHz at 0°. The spectral maximum also shifted to higher frequencies and increased by nearly 10 dB in amplitude. As the RBC diameter increased, at 90° the spectral minima shifts from 220 MHz for a 7.82 µm diameter RBC to 280 for a 6.8 µm diameter RBC.

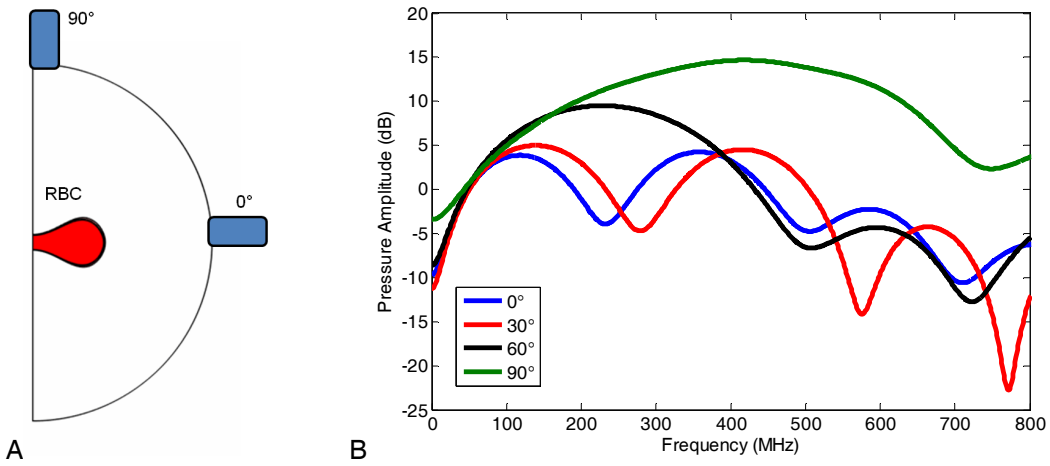


Figure 3. (A) A schematic of the FEM with the RBC at the center with the locations at which pressure was recorded (emulating the relative orientation of the transducers and red blood cell in the experiment). (B)The power spectrum of the photoacoustic signal recorded at angles of 0°, 30°, 60° and 90° relative to the RBC.

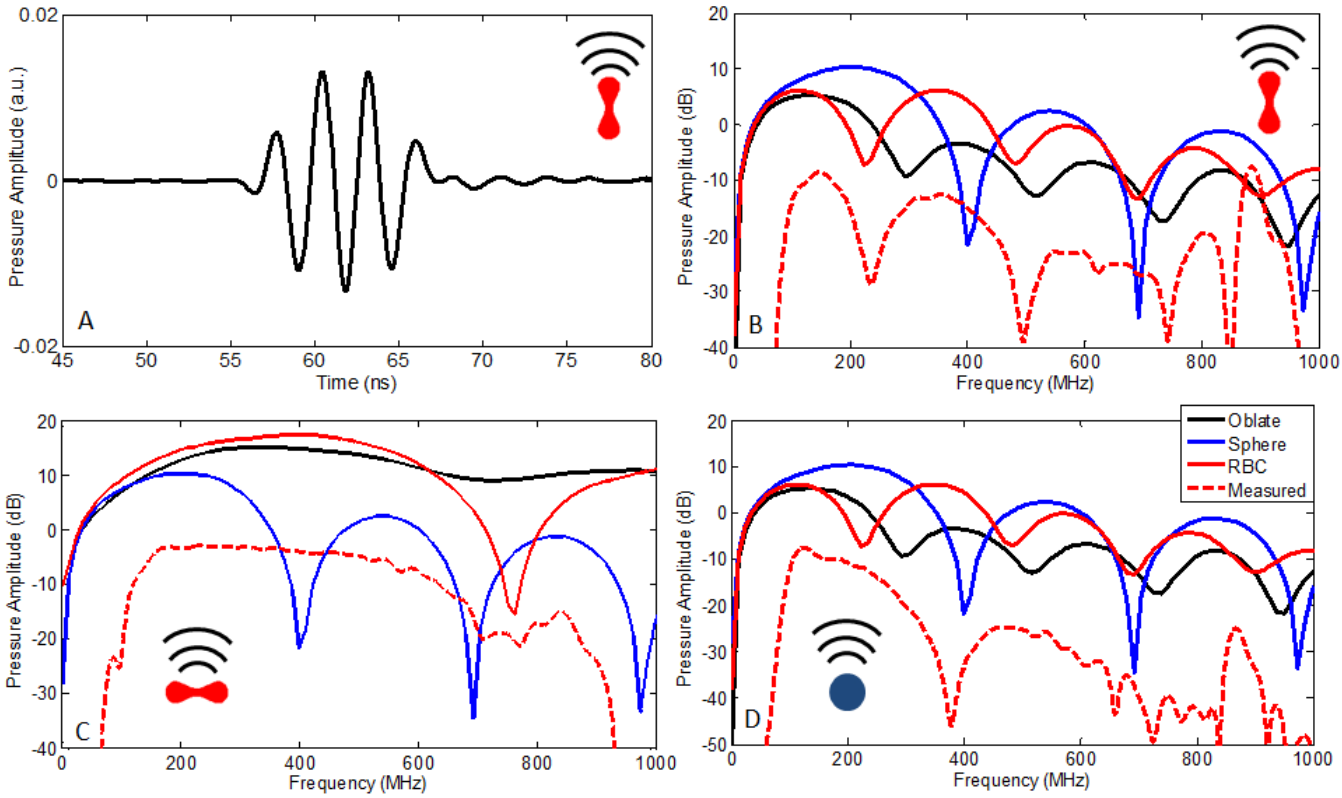


Figure 4. The measured photoacoustic signals and numerical simulations of RBCs. (A) The measured photoacoustic signal from a single 8 μm diameter RBC in a vertical orientation. (B) The photoacoustic power spectrum of the RBC in a vertical orientation and (C) in a horizontal orientation relative to the transducer. (D) The photoacoustic power specturm of a 5.8 μm diameter RBC. For (B-D), the measured signal is indicated by the red dotted line, which is compared to the oblate (solid black line), spherical (solid blue line) and biconcave shape (solid red line) numerical simulations. Good agreement between the measured signal and their respective shape was observed. The measured RBC shape and orientation relative to the transducer is inset within each graph.

A RBC with a diameter of 8 μm (determined optically) was measured at 0°, then again at 90° after it rotated to a horizontal orientation. The power spectrum for the 0° and 90° orientation are shown in figure 4. While the -6 dB bandwidth of the 375 MHz transducer is 42%, it can detect signals from approximately 150 to 550 MHz provided the SNR is large enough. For the RBC measured at 0° (on its edge), distinct spectral minima were observed at 220 and 500 MHz. These spectral locations agree with those predicted using the FEM model. In comparison, the spectrum of the oblate and spherical models is also shown in figure 4, where poor agreement to the measured signal is observed. For the RBC measured at 90° (flat), the measured signal lacks any specific spectral features throughout the transducer bandwidth (figure 4). The first spectral minimum occurs at 800 MHz, which is well outside the bandwidth for this transducer. The measured spectrum agrees well with both the oblate and biconcave shape models.

Photoacoustic signals from RBCs placed in a hypotonic solution were then measured. Water was added to the cell culture medium to reduce the osmolarity from approximately 300 mosms/L to 100 mosms/L, which induced swelling within the RBC. The diameter of the RBC was determined using optical imaging to be 5.6 μm and was roughly spherical. The power spectrum from this RBC is shown in figure 4. The spectral minimum occurs at 390 MHz, which agrees with the spherical model.

As shown in figure 4, for RBC simulations with photoacoustic frequencies over 100 MHz, it is important that the correct RBC shape is used for accurate results. However when using frequencies less than 100 MHz, the power spectrum for all three models is similar, and decreases gradually with decreasing frequency. The signal decreases rapidly below 20 MHz, dropping 15 dB from 20 to 5 MHz. Photoacoustic microscopy systems generally use frequencies from 10 to 40 MHz, therefore approximating the bi-concave shape as an oblate or sphere may be suitable for simulations using single or dilute suspensions of RBCs.

## IV. Conclusions

This paper demonstrates how quantitative photoacoustic methods can be used to infer the size and orientation of single RBCs using frequencies over 100 MHz. Previously our research group has shown that photoacoustic frequencies above 100 MHz can be used to identify and size spherically symmetric nanoparticle-loaded micron-sized perfluorocarbon droplets [15]. Periodically varying minima and maxima were observed throughout the power spectrum that are unique to the size, shape and composition of the object. These spectral features generally occur above 100 MHz for micron-sized objects. The methods presented can be applied to any particle provided sufficient optical absorption occurs at the irradiating wavelengths and will be applied towards measurements of single cells.

## Acknowledgment

E. Strohm and E. Hysi are supported through NSERC scholarships. This research was undertaken, in part, thanks to funding from the Canada Research Chairs Program awarded to M. Kolios. Funding to purchase the equipment was provided by the Canada Foundation for Innovation, the Ontario Ministry of Research and Innovation, and Ryerson University.

## References

[1] E. Evans and Y.-C. Fung, "Improved measurements of the erythrocyte geometry," *Microvascular Research*, vol. 4, no. 4, pp. 335–347, Oct. 1972.

[2] M. M. Wintrobe, J. P. Greer, and G. R. Lee, *Wintrobe's clinical hematology*. Philadelphia: Wolters Kluwer/Lippincott Williams & Wilkins, 2009.

[3] D. Cojoc, S. Finaurini, P. Livshits, E. Gur, A. Shapira, V. Mico, and Z. Zalevsky, "Toward fast malaria detection by secondary speckle sensing microscopy," *Biomed Opt Express*, vol. 3, no. 5, pp. 991–1005, Apr. 2012.

[4] L. Golan, D. Yeheskely-Hayon, L. Minai, E. J. Dann, and D. Yelin, "Noninvasive imaging of flowing blood cells using label-free spectrally encoded flow cytometry," *Biomed. Opt. Express*, vol. 3, no. 6, pp. 1455–1464, Jun. 2012.

[5] Cloutier G. and Qin Z., "Ultrasound backscattering from non-aggregating and aggregating erythrocytes-a review," *Biorheology*, vol. 34, no. 6, p. 443, 1997.

[6] K. Maslov, H. F. Zhang, S. Hu, and L. V. Wang, "Optical-resolution confocal photoacoustic microscopy," in *Proceedings of SPIE*, 2008, vol. 6856, p. 68561I–68561I–7.

[7] Y. Yuan, S. Yang, and D. Xing, "Optical-resolution photoacoustic microscopy based on two-dimensional scanning galvanometer," *Applied Physics Letters*, vol. 100, no. 2, pp. 023702–023702–3, Jan. 2012.

[8] G. J. Diebold, M. I. Khan, and S. M. Park, "Photoacoustic 'Signatures' of Particulate Matter: Optical Production of Acoustic Monopole Radiation," *Science*, vol. 250, no. 4977, pp. 101–104, Oct. 1990.

[9] A. S. Ahuja and W. R. Hendee, "Effects of red cell shape and orientation on propagation of sound in blood," *Medical Physics*, vol. 4, no. 6, pp. 516–520, 1977.

[10] R. K. Saha and M. C. Kolios, "Effects of erythrocyte oxygenation on optoacoustic signals," *Journal of Biomedical Optics*, vol. 16, no. 11, p. 115003, 2011.

[11] E. M. Strohm, G. J. Czarnota, and M. Kolios, "Quantitative measurements of apoptotic cell properties using acoustic microscopy," *IEEE Trans. Ultrason., Ferroelectr., Freq. Control*, vol. 57, no. 10, pp. 2293–2304, 2010.

[12] E. M. Strohm, M. Rui, I. Gorelikov, N. Matsuura, and M. Kolios, "Vaporization of perfluorocarbon droplets using optical irradiation," *Biomedical Optics Express*, vol. 2, no. 6, pp. 1432–1442, 2011.

[13] W. H. Grover, A. K. Bryan, M. Diez-Silva, S. Suresh, J. M. Higgins, and S. R. Manalis, "Measuring single-cell density," *PNAS*, vol. 108, no. 27, pp. 10992–10996, Jul. 2011.

[14] A. S. Dukhin, P. J. Goetz, and T. G. M. van de Ven, "Ultrasonic characterization of proteins and blood cells," *Colloids and Surfaces B: Biointerfaces*, vol. 53, no. 2, pp. 121–126, Dec. 2006.

[15] E. M. Strohm, I. Gorelikov, N. Matsuura, and M. C. Kolios, "Acoustic and photoacoustic characterization of micron-sized perfluorocarbon emulsions," *J. Biomed. Opt*, vol. 17, no. 9, pp. 096016–1–9, Sep. 2012.